COMMUNICATIONS CHEMISTRY

ARTICLE

DOI: 10.1038/s42004-017-0006-7 OPEN

Coherent vibrations in methanol cation probed by periodic H_3^+ ejection after double ionization

Toshiaki Ando[1], Akihiro Shimamoto[1], Shun Miura[1], Atsushi Iwasaki[1], Katsunori Nakai[1] & Kaoru Yamanouchi[1]

When hydrocarbon molecules are exposed to an intense laser field, triatomic hydrogen molecular ion, H_3^+, is ejected. Here we describe pump–probe measurements of the ejection of H_3^+ from methanol dication with high temporal resolution using intense few-cycle laser pulses and find a long-lasting periodic increase in the yield of H_3^+. We show that H_3^+ ejection is the lowest energy decomposition channel and that its yield is enhanced each time when the vibrational wave packet coming back to the inner turning point of methanol cation is projected onto the dication potential energy surface. We also show that the time-resolved measurement of the yield of H_3^+ is an efficient tool not only for probing ultrafast nuclear dynamics of hydrocarbon cations but also for deriving vibrational frequencies of hydrocarbon cations with high precision.

[1] Department of Chemistry, School of Science, The University of Tokyo, 7-3-1 Hongo, Bunkyo-ku, Tokyo 113-0033, Japan. Correspondence and requests for materials should be addressed to K.Y. (email: kaoru@chem.s.u-tokyo.ac.jp)

It has been shown that triatomic hydrogen molecular ion, H_3^+, plays an important role in interstellar chemistry[1]. For example, H_3^+ formed through a bimolecular reaction, $H_2^+ + H_2 \rightarrow H_3^+ + H$, can protonate a neutral molecule X by a subsequent bimolecular collision, $H_3^+ + X \rightarrow HX^+ + H_2$, which may lead to further subsequent interstellar chemical reactions. It has also been shown that H_3^+ can be emitted from hydrocarbon molecular dication prepared by electron impact ionization[2], by extreme ultraviolet photoionization[3], and by irradiation of intense femtosecond laser pulses[4–6]. The formation of H_3^+ from allene[7–9] and the formation of HD_2^+ from CD_3OH[10] showed that migration of hydrogen atoms can proceed in the formation of H_3^+. Recently, we interpreted the mechanism of H_3^+ formation from dication of methanol theoretically as a unimolecular decomposition process in which a long-lived neutral moiety of H_2, formed within a dication molecule, abstracts a proton in the other moiety having the charge of +2[11]. Through a series of our studies on the formation of H_3^+ from hydrocarbon molecules by the irradiation of ultrashort intense laser pulses[7,10,12–14], we showed that the hydrocarbon dications from which H_3^+ is ejected are all long lived, and that their lifetimes are comparable to or longer than a period of the overall rotation of the dications. These findings mean that the intramolecular vibrational-energy redistribution proceeds to a large extent within the energized dications prior to the ejection of H_3^+.

When hydrocarbon dication is prepared by sequential ionization from neutral by two ultrashort laser pulses, the vibrational energy of the dication is varied depending on the delay time of the second ionization pulse with respect to the first ionization pulse that prepares a vibrational wave packet on the potential energy surface of the monocation, reflecting the temporal evolution of the wave packet. Therefore, if we monitor the ejection of H_3^+ from the dication in real time, we will be able to explore ultrafast nuclear dynamics of hydrocarbon molecules at the monocation stage by taking advantage of the existence of the long-lived dication, acting as an energized state in the unimolecular dissociation.

In the present study, we record the yield of H_3^+ produced from methanol dication,

$$CH_3OH^{2+} \rightarrow CHO^+ + H_3^+, \qquad (1)$$

in time domain by the pump–probe coincidence momentum imaging (CMI) method using near-infrared few-cycle laser pulses whose pulse duration is 6 fs and monitor the vibrational motion of CH_3OH^+ with high temporal resolution of as high as ~6 fs.

Results

Origin of periodic ejection of H_3^+. Figure 1a shows the distribution of the released kinetic energy, E_{kin}, and the ion yield of the two-body Coulomb explosion pathway (1) as a function of the pump–probe time delay Δt. The ion yield exhibits a periodic increase with the period of ~38 fs starting from $\Delta t \sim 58$ fs, and this periodic structure continues beyond 500 fs as seen in Fig. 1b. The temporal pulse profiles of the few-cycle laser pulses employed in the present experiment are shown in Supplementary Figure 1. In order to extract the frequency of the ion yield oscillation, we perform the Fourier transform of the yield in the range of $120 < \Delta t < 500$ fs in Fig. 1b, and obtain Fig. 1c, in which a distinct peak appears at ~26.3 THz, corresponding to the period of ~38.0 fs. This long-lasting oscillation can only be ascribed to the motion of the vibrational wave packet on the electronic ground state of CH_3OH^+ because even the lowest electronically excited state of CH_3OH^+ is located 0.5 eV above the dissociation threshold for $CH_2OH^+ + H$[15,16] and the wave packet prepared on these electronically excited states is expected to decay into the dissociation continuum.

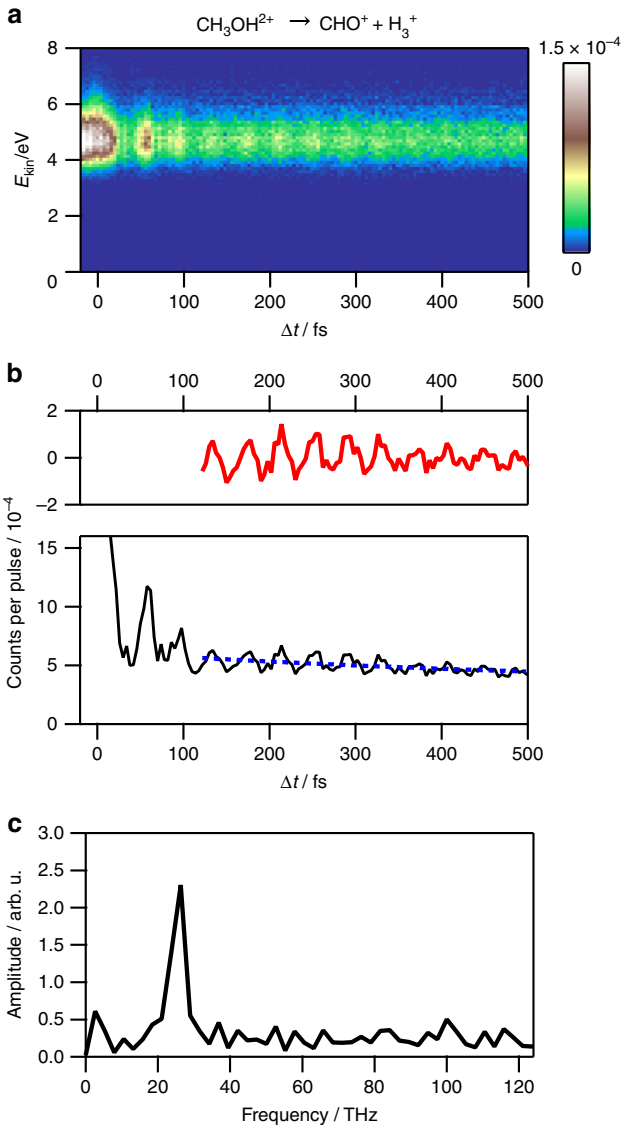

Fig. 1 The ion yield of H_3^+ ejection pathway. **a** The E_{kin} distribution of the H_3^+ ejection Coulomb explosion pathway (1). **b** The ion yields of the H_3^+ ejection Coulomb explosion pathway (1). Black curve: ion yield as a function of the Δt. Blue broken curve: optimized exponential curve to which the ion yield data are fitted in the time range between $\Delta t = 120$ fs and 500 fs. Red curve: residual ion yield after the subtraction of the optimized exponential curve. **c** The Fourier-transformed ion yields of the H_3^+ ejection pathway (1) using the data in the range of $120 < \Delta t < 500$ fs

This frequency is closed to the C-O stretching frequency 26.8 THz (895 cm^{-1}) of the electronic ground state of CH_3OH^+[15].

It is known from photoion–photoion coincidence measurement[17] that the H_3^+ ejection pathway (1) and the H^+ ejection pathway

$$CH_3OH^{2+} \rightarrow CH_3O^+ + H^+, \qquad (2)$$

have the lowest threshold energies among all the possible decomposition pathways of CH_3OH^{2+}. The decomposition pathway having the next lowest threshold energy is the H_2^+ ejection pathway,

$$CH_3OH^{2+} \rightarrow CH_2O^+ + H_2^+, \qquad (3)$$

whose threshold energy is located at ~0.5 eV higher than the pathways (1) and (2)[17], and the decomposition pathway having

the second next lowest threshold energy is the three body explosion pathway,

$$CH_3OH^{2+} \rightarrow CHO^+ + H^+ + H_2, \quad (4)$$

whose threshold energy is located at ~1 eV higher than the pathways (1) and (2)[17].

From the number of events at Δt ~500 fs in the high E_{kin} region above 3.5 eV, the relative yields of the pathways (1), (2), (3), and (4) in our measurements are derived to be 1:1:0.07:3.6, respectively, showing that the three body explosion pathway (4) has the largest ion yield and the pathway (3) is a minor pathway.

Considering that the period of ~38 fs identified in Fig. 1c in time domain is in good agreement with the vibrational frequency of the CO stretching mode of the electronic ground state of CH_3OH^+, we plot the schematic potential energy curves of the electronic ground state of CH_3OH ($\tilde{X}^1A'$), CH_3OH^+ $((2a'')^{-1}$ $\tilde{X}^2A'')$, and CH_3OH^{2+} $((2a'')^{-2}\tilde{X}^1A')$ along the CO stretching coordinate in Fig. 2. According to previous experimental and theoretical studies, the equilibrium C-O internuclear distances of CH_3OH, CH_3OH^+, and CH_3OH^{2+} are 1.428(3) Å[18] 1.36 Å[19], and 1.19 Å[19], reflecting the fact that the 2a" orbital has an anti-bonding character, and therefore, upon the first ionization, the vibrational wave packet is expected to be prepared at the outer turning point of the potential energy curve. Consequently, as the delay time increases, the energy of the dication decreases and takes the minimum value at $\Delta t = 19$ fs, a half of the vibrational period of the CO stretch of the monocation, and then the energy becomes maximum at $\Delta t = 38$ fs. The delay times at which the yield of H_3^+ became maximum, 58 fs, 96 fs, 134 fs…, shown in Fig. 1a, correspond to the timings when the vibrational wave packet reached the inner turning point of the potential energy curve of the monocation, i.e., the timing when the energy of the dication takes the minimum value. Therefore, it is probable that, at the lowest energy of the dication, only the lowest energy channels (1) and (2) are open energetically, and that once the other dissociation channels are opened energetically, they dominate over the lowest energy channels, leading to the decrease in the yield of H_3^+ through the channel (1).

Unimolecular decomposition of CH_3OH^{2+}. In order to discuss more precisely the unimolecular decomposition leading to the periodic ejection of H_3^+, we explored the multi-dimensional potential energy surface of CH_3OH^{2+} by density functional theory calculations to find the transition states for the dissociation pathways. As plotted in Fig. 3, there are two transition states, TS1a (0.56 eV) and TS1b (0.85 eV), in the H_3^+ ejection pathway (1). At TS1a and TS1b, CH_3OH^{2+} takes two different characteristic geometrical structures, both of which show that neutral H_2 is attached to $CHOH^{2+}$ moiety. These two transition state structures at TS1a and TS1b, representing a loosely bound complex in which the charge induced dipole moment of the H_2 moiety is bound by the positive charge of the $CHOH^{2+}$ moiety. When the unimolecular reaction proceeds through TS1a, H_3^+ is expected to be ejected from methyl group, and, when it proceeds through TS1b, H_3^+ is expected to be ejected from hydroxyl group after the migration of neutral H_2 from methyl group as was discussed in ref. [11]. The energy of the transition state of the pathway (2) (TS2), 0.65 eV, is located between the energies of TS1a and TS1b.

As shown in Fig. 4, the yield of the pathway (2) as a function of the pump–probe delay also exhibits the oscillatory structure similar to the one shown in Fig. 1b for the pathway (1). Even though the yield of the pathway (2) is almost the same as the yield of the pathway (1), the amplitude of the oscillation of the pathway (2) is found to be only one third of that of the pathway (1).

This larger oscillation amplitude in the pathway (1) can be discussed by the Rice–Ramsperger–Kassel–Marcus (RRKM) unimolecular reaction theory. The spontaneous reaction rate $k_2(E)$ in the RRKM theory[20] can be written as

$$k_2(E) = \frac{W^{\ddagger}(E - E_0)}{h\rho(E)}, \quad (5)$$

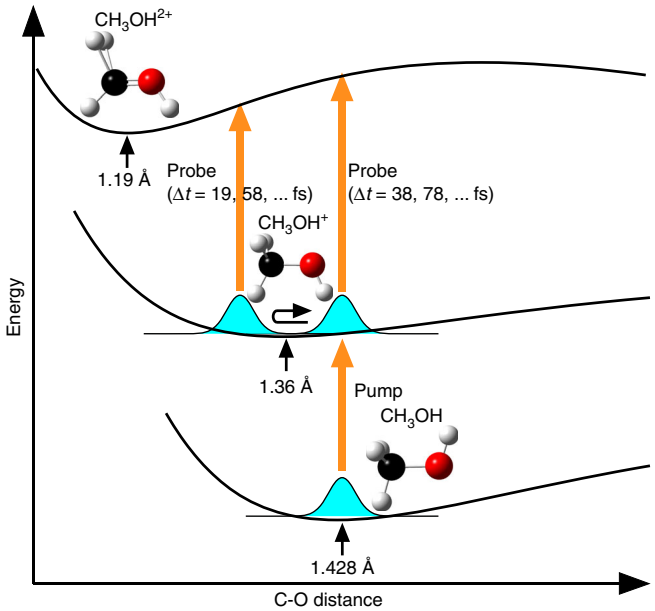

Fig. 2 Schematics of the potential energy curves along the CO internuclear distance. The vibrational wave packet of CH_3OH^+ prepared by the first laser pulse at the outer turning point starts moving towards the shorter internuclear distance region and the oscillation continues. The wave packet prepared in CH_3OH^{2+} by the second laser pulse has the lowest energy every time when the wave packet of CH_3OH^+ comes back to the inner turning point periodically with the interval of 38 fs starting from at $\Delta t = 19$ fs

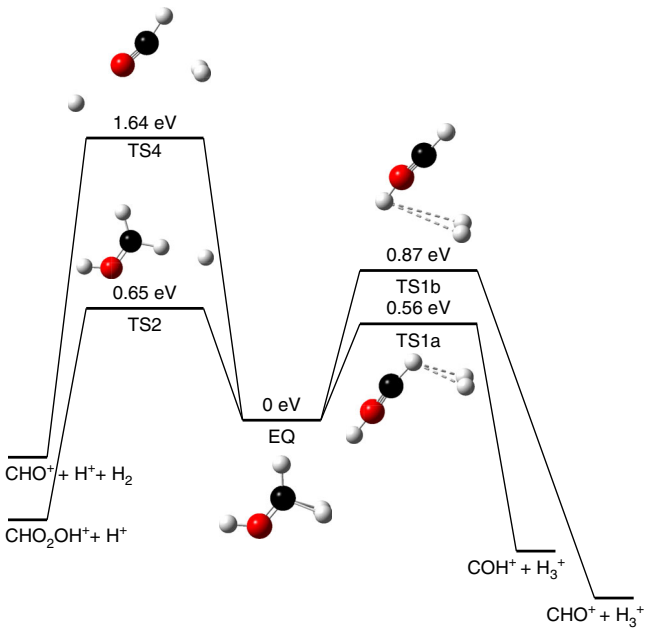

Fig. 3 Theoretical energy diagram of CH_3OH^{2+}. The zero point energies at the three transition states (TS1a, TS1b, TS2, and TS4) measured from the zero point energy at the equilibrium structure (EQ) are shown

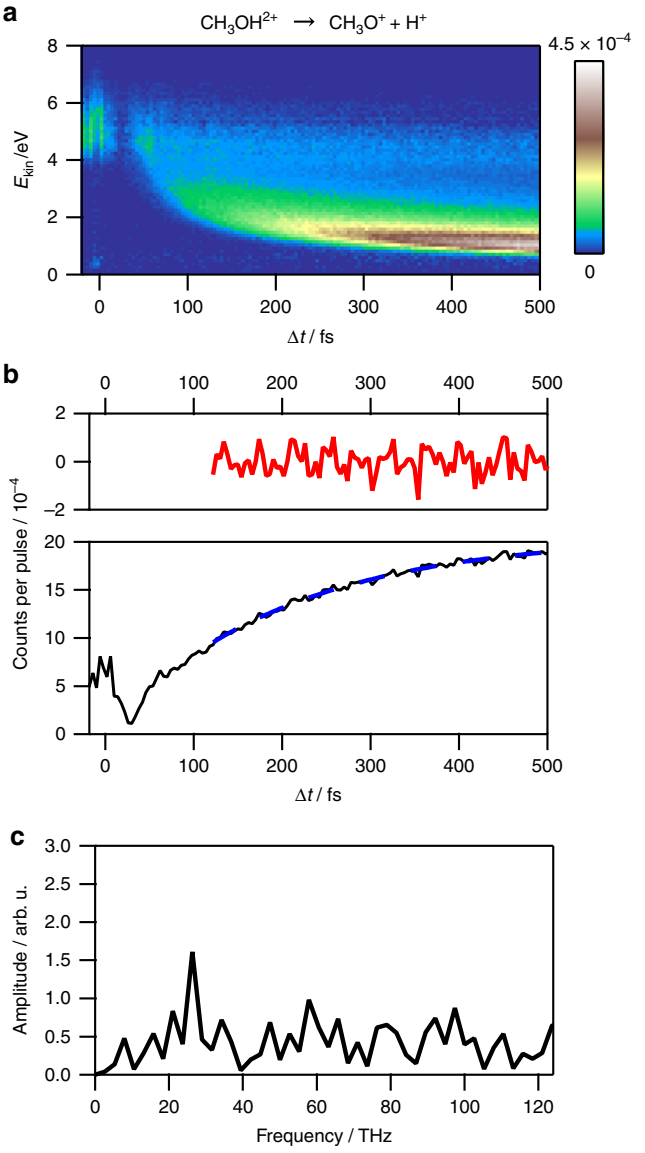

Fig. 4 The ion yield of H^+ ejection pathway. **a** The E_{kin} distribution of the H^+ ejection Coulomb explosion pathway (2). **b** The ion yields of the H^+ ejection Coulomb explosion pathway (2). Black curve: ion yield in the high E_{kin} region above 3.5 eV as a function of the Δt. Blue broken curve: optimized exponential curve to which the ion yield data are fitted in the time range between 120 and 500 fs. Red curve: residual ion yield after the subtraction of the optimized exponential curve. **c** The Fourier-transformed ion yields of the H^+ ejection pathway (2) using the data in the range of $120 < \Delta t < 500$ fs

where E and E_0 are the internal energy for the parent dication and the zero point energy for the TS, respectively, $W^{\ddagger}$ is the number of the energetically allowed vibrational levels for the vibrational motion along the directions perpendicular to the reaction coordinate at the transition state, and $\rho(E)$ is the density of states of the parent dication. Since $\rho(E)$ is common in these two pathways (1) and (2), the difference in the yield can be ascribed to the difference in $W^{\ddagger}$. This means that when the difference between the threshold energy for H_3^+ production and that for the H^+ production is small, their relative yield is governed by the $W^{\ddagger}$ values.

We calculated the vibrational frequencies of the vibrational modes at TS1a, TS1b, and TS2 as shown in Supplementary Table 1, and evaluated $W^{\ddagger}$ as a function of E–E_0. The results are

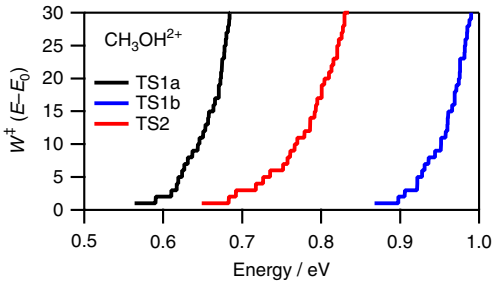

Fig. 5 The numbers of energetically allowed vibrational levels at the TSs of CH_3OH^{2+}. The $W^{\ddagger}$ at TS1a (black), TS1b (blue), and TS2 (red) are counted by the Beyer Swinhart algorithm[29] as a function of the internal energy, which is measured from the zero point energy at the EQ of CH_3OH^{2+}

plotted in Fig. 5, showing that $W^{\ddagger}$ at TS1a and TS1b increases more rapidly than $W^{\ddagger}$ at TS2, which can be ascribed to the difference in the numbers of the low-frequency vibrational modes at these three transition states. The numbers of the vibrations modes having the lower wavenumber than 600 cm^{-1} are six and five at TS1a and TS1b, respectively, while the number at TS2 is only two. The larger number of the low-frequency vibrational modes contribute to the increase in $W^{\ddagger}$ at TS1a and TS1b. Among these low-frequency vibrational modes, the vibrational mode (215 cm^{-1}) assigned to the rotation of the H_2 loosely bound neutral moiety at TS1a and the corresponding vibrational mode (242 cm^{-1}) at TS1b contribute largely to the more rapid increase in $W^{\ddagger}$ at these two transition states than the increase in $W^{\ddagger}$ at TS2.

It may be said that TS1b could not contribute in the competition between the pathway (1) and the pathway (2) because the energy of TS1b is 0.31 eV higher than the energy of TS1a. However, within the accuracy of the theoretical calculations, it is difficult to judge if such a small energy difference is accurately evaluated. Therefore, we regard that both TS1a and TS1b are located closely in energy to TS2 in this threshold region of the two decomposition pathways and that the more rapid increase in $W^{\ddagger}$ at TS1a and TS1b than $W^{\ddagger}$ at TS2 results in the more rapid increase in the spontaneous reaction rate for the H_3^+ ejection pathway (1) than that for the H^+ ejection pathway (2), which explains the reason why the observed amplitude for the oscillation in the H_3^+ ejection pathway is about three times as large as that in the H^+ ejection pathway, i.e., the pathway (2).

It is known that the ejection of H^+ through the pathway (2) proceeds very rapidly within the time range of 70–290 fs[13]. Therefore, it is probable that the large portion of H^+ are produced via the pathway (2) from the precursor dications prepared in a much higher energy region above TS2, resulting in the non-oscillating components seen in Fig. 4, and that the small portion of the wave packet prepared in the low energy region slightly above TS2 contribute to the oscillating component in the pathway (2).

Mechanism of H_3^+ and H_2D^+ ejections from CH_3OD^{2+}. In order to confirm our discussion above, we have also performed pump–probe CMI measurements of partially deuterated methanol, CH_3OD, for the H_3^+ ejection pathway from CH_3OD^{2+},

$$CH_3OD^{2+} \rightarrow COD^+ + H_3^+, \quad (6)$$

proceeding via TS1a, and the H_2D^+ ejection pathway,

$$CH_3OD^{2+} \rightarrow CHO^+ + H_2D^+, \quad (7)$$

proceeding via TS1b.

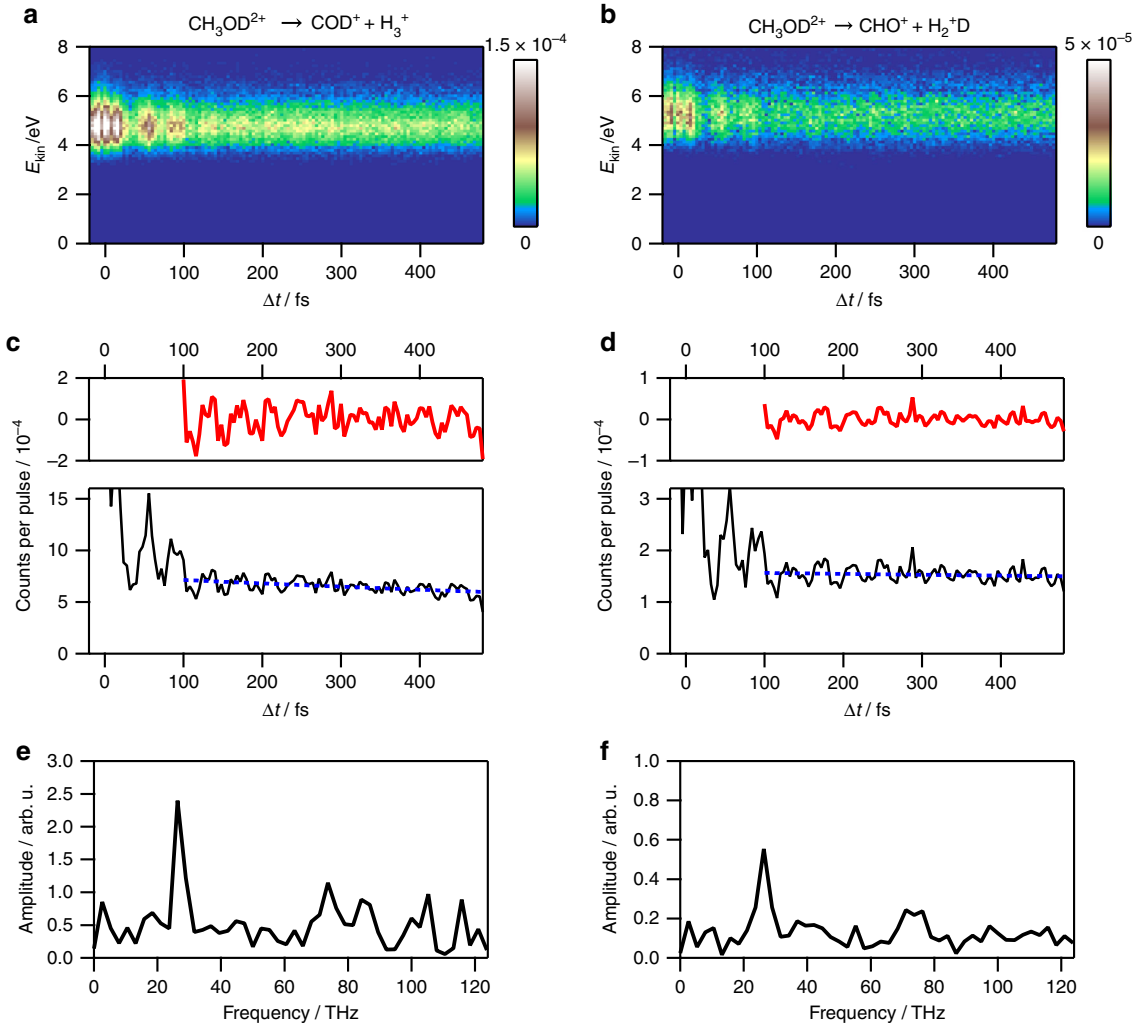

Fig. 6 The ion yield of H_3^+ and H_2D^+ ejection pathway from CH_3OD^{2+}. The E_{kin} distribution of the H_3^+ ejection pathway (6) (**a**) and the H_2D^+ ejection pathway (7) (**b**) from CH_3OD^{2+}. The ion yields of the H_3^+ ejection pathway (6) (**c**) and the H_2D^+ ejection pathway (7) (**d**). Black curve: ion yield as a function of the Δt. Blue broken curve: optimized exponential curve to which the ion yield data are fitted in the time range between $\Delta t = 100$ fs and 480 fs. Red curve: residual ion yield after the subtraction of the optimized exponential curve. The Fourier-transformed ion yields of the H_3^+ ejection pathway (6) (**e**) and the H_2D^+ ejection pathway (7) (**f**) using the data in the range of $100 < \Delta t < 480$ fs

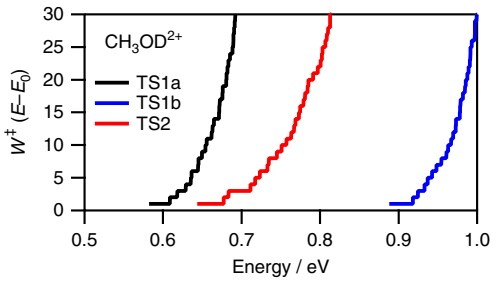

Fig. 7 The numbers of energetically allowed vibrational levels at the TSs. The $W^{\ddagger}$ at TS1a (black), TS1b (blue), and TS2 (red) are counted by the Beyer Swinhart algorithm[29] as a function of the internal energy, which is measured from the zero point energy at the EQ of CH_3OD^{2+}

As shown in Fig. 6, both of the ion yield of the pathway (6) and that of the pathway (7) exhibit periodic peak structures with a common period of 26.3(26) THz, which agrees well with the frequency of the C-O stretching that is 27.8(9) THz (928(30) cm^{-1})[21]. As shown in Fig. 6e, f, the oscillation amplitude of the pathway (7) via TS1b is around one fourth of the pathway (6) via TS1a, suggesting that the two pathways compete and their threshold energies are located closely to each other even though TS1b is expected to be somewhat higher in energy than TS1a.

The number of the energetically allowed levels $W^{\ddagger}$ of CH_3OD^{2+} at TS1a and that at TS1b are calculated as shown in the Fig. 7. Even though the $W^{\ddagger}$ values at the two transition states increases rapidly in a similar manner, the threshold energy for TS1b is about 0.3 eV higher than that for TS1a. The observation that the dissociation pathways (6) and (7) compete shows the energy difference between TS1a and TS1b is overestimated by about 0.3 eV in the calculation. The experiment using the partially deuterated methanol, CH_3OD, has revealed that H_3^+ ejection can proceed through both of the transition states, TS1a and TS1b, and that TS1b is only slightly (<0.1 eV) higher in energy than TS1a.

The pathway (4) has the largest yield among these pathways, indicating that a large portion of CH_3OH^{2+} is prepared in the higher internal energy than the threshold energy of the pathway (4). As shown in Fig. 8, no long-lasting periodic peak structure can be seen in the yield of the pathway (4), indicating that the periodic dip in the yield of the pathway (4) that should be associated with the increase in the yields of the pathways (1) and

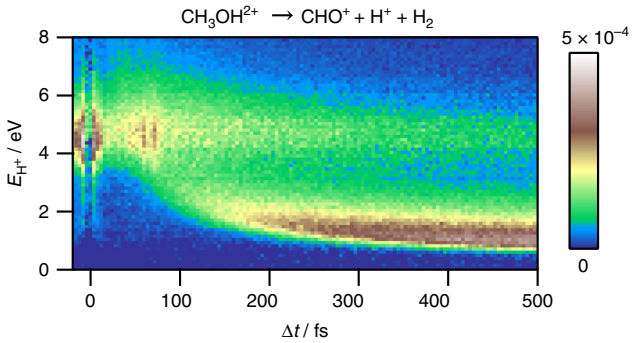

Fig. 8 The three body explosion pathway (4). The distribution of the kinetic energy of H^+ generated through the three body explosion pathway (4). The strong signal with a vertical stripe at $\Delta t \sim 70$ fs is ascribed to the optical interference between the satellite structure of one of the pump and probe laser pulses and the main central part of the other laser pulse

(2) is so small in its magnitude compared with the total yield of the pathway (4).

We have found the periodic increase in the yield of H_3^+ from CH_3OH^{2+} and that of H_3^+ and H_2D^+ from CH_3OD^{2+}, lasting for as long as 500 fs or more by the pump–probe measurement with the temporal resolution as high as 4–6 fs, and demonstrated that the period (~38 fs) of the C-O stretching vibration of methanol monocation can be obtained from the Fourier transform of the time-resolved signals.

Because methanol dication from which H_3^+ is ejected is long lived, unimolecular reaction theory have been applied to the decomposition process. By evaluating the spontaneous reaction rate for the H_3^+ decomposition pathway by the RRKM unimolecular reaction theory, we have found that the loose transition states having the low-frequency vibrational modes play a crucial role in guiding the dication towards the H_3^+ ejection pathway.

The H_3^+ ejection from hydrocarbon dications can be regarded as a general phenomenon for hydrocarbon molecules having more than two hydrogen atoms[4]. It is possible that H_3^+ ejection from other hydrocarbon dication species proceeds also through this type of loose transition state. Because the energized state is regarded as the dense manifold of the vibrational levels to which the wave packet motion of monocation is to be projected, time-resolved monitoring of the very slow H_3^+ ejection process and its Fourier transform can be a useful spectroscopic method for determining the vibrational frequencies of hydrocarbon cations that are difficult to be obtained by conventional spectroscopic methods. The time-resolved detection of H_3^+ from methanol dication induced by the intense field sequential ionization have given us an opportunity to investigate the vibrational dynamics of methanol cation.

Methods

Experimental apparatus. The details of our experimental setup have been described in the previous report[22]. Briefly, few-cycle laser pulses were generated by a hollow-core fiber compression technique using an output of a chirped pulse amplification femtosecond Ti:sapphire laser system (800 nm, 5 kHz, 0.6 mJ, 30 fs). The few-cycle laser pulses were introduced into a Michelson interferometer to generate pump and probe pulses. The optical time delay Δt between the pump and probe laser pulses was varied in the range between around −20 fs and 500 fs using a piezo-controlled optical stage. The pulse duration was measured to be 6.0 fs and the center wavelength was 770 nm for CH_3OH. In the experiment of CH_3OD, the pulse was compressed so that the duration became 4.4 fs and the center wavelength was 770 nm. Both the pump and probe laser pulses were focused onto an effusive molecular beam of methanol in a vacuum chamber by a concave mirror ($f = 150$ mm). The laser polarization direction of the pump laser pulses and that of the probe laser pulses were set to be parallel to the propagation axis of the molecular beam. The focal intensity was estimated to be 2.1×10^{14} W cm^{-2} for CH_3OH and 2.7×10^{14} W cm^{-2} for CH_3OD. The temporal shapes of the few-cycle laser pulses were measured by the method of two-dimensional spectral shearing interferometry[23] and shown in Supplementary Figure 1.

The fragment ions generated from methanol were guided by static electric fields toward a two-dimensional position sensitive detector (HEX120, RoentDek) in the velocity map imaging configurations. From the flight times of the fragment ions and the positions on the detector plane where the fragment ions hit, the momentum vectors of the fragment ions were determined. Events of the two-body Coulomb explosion pathways were extracted by the CMI method[24]. The released kinetic energy E_{kin} was plotted as a function of the time delay Δt in the delay time range of −20 to 500 fs with delay increment step of 4 fs. Events of the three body explosion pathway (4) were extracted by the covariance mapping method[25].

Extraction of pump–probe signals. The row data of E_{kin} distributions of the dissociation pathways include the signals generated by the pump laser pulse only and those generated by the probe laser pulse only because methanol dication can also be generated by a single laser pulse. The E_{kin} distribution $Y_{diff}(E_{kin},\Delta t)$ generated from methanol dication prepared exclusively by the sequentially ionization by the pump and probe laser pulses, which is shown for example in Fig. 1a for the dissociation pathway (1), was derived by subtracting the signals generated by the pump laser pulse only $Y_{pump}(E_{kin})$ and those generated by the probe laser pulse only $Y_{probe}(E_{kin})$ from the E_{kin} distributions $Y_{pump\text{-}probe}(E_{kin}, \Delta t)$ as

$$Y_{diff}(E_{kin}, \triangle t) = Y_{pump-probe}(E_{kin}, \triangle t) - (Y_{pump}(E_{kin}) - \alpha Y_{probe}(E_{kin})), \quad (8)$$

where α is a correction factor describing a depletion of sample molecules by irradiating the pump laser pulse. As the value of α, $\alpha = 0.79(5)$ was adopted for CH_3OH, which was obtained in ref. [22] by comparing the total ion yield obtained by the pump laser pulse only, by the probe laser pulse only, and by the pump and probe laser pulses. For CH_3OD, the lower value α, $\alpha = 0.4$, was adopted for CH_3OD because the sample is depleted to a larger extent associated with the larger laser pulse intensity.

Geometrical structures of CH_3OH^{2+} at TSs and EQ. The geometry optimization of the transition states and the equilibrium structures were performed using the global reaction route mapping (GRRM1.2) program[26–28] using energies and gradient vectors computed by the Gaussian09 program with the density functional theory at the UB3LYP/aug-cc-pVTZ level after exploring transition states and equilibrium structures with UB3LYP/6-31G(d) level.

Data availability. The data that support the findings of this study are available from the corresponding author upon reasonable request.

Received: 28 November 2017 Accepted: 13 December 2017
Published online: 08 March 2018

References

1. Oka, T. & Jagod, M. F. Infrared spectrum of H_3^+ as an astronomical probe. *J. Chem. Soc. Faraday Trans.* **89**, 2147–2154 (1993).
2. Wang, P. & Videl, C. R. Dissociation of multiply ionized alkanes from methane to *n*-butane due to electron impact. *Chem. Phys.* **280**, 309–329 (2002).
3. Eland, J. H. D. The origin of primary H_3^+ in mass spectra. *Rapid Commun. Mass. Spectrom.* **10**, 1560–1562 (1996).
4. Hoshina, K., Furukawa, Y., Okino, T. & Yamanouchi, K. Efficient ejection of H_3^+ from hydrocarbon molecules induced by ultrashort intense laser fields. *J. Chem. Phys.* **129**, 104302 (2008).
5. Kraus, P. M. et al. Unusual mechanism for H_3^+ formation from ethane as obtained by femtosecond laser pulse ionization and quantum chemical calculations. *J. Chem. Phys.* **134**, 114302 (2011).
6. Ekanayake, N. et al. Mechanisms and time-resolved dynamics for trihydrogen cation (H_3^+) formation from organic molecules in strong laser fields. *Sci. Rep.* **7**, 4703 (2017).
7. Xu, H., Okino, T. & Yamanouchi, K. Ultrafast hydrogen migration in allene in intense laser fields: evidence of two-body Coulomb explosion. *Chem. Phys. Lett.* **469**, 255–260 (2009).
8. Mebel, A. M. & Bandrauk, A. D. Theoretical study of unimolecular decomposition of allene cations. *J. Chem. Phys.* **129**, 224311 (2008).
9. Kübel, M. et al. Steering proton migration in hydrocarbons using intense few-cycle laser fields. *Phys. Rev. Lett.* **116**, 193001 (2016).
10. Furukawa, Y., Hoshina, K., Yamanouchi, K. & Nakano, H. Ejection of triatomic hydrogen molecular ion from methanol in intense laser fields. *Chem. Phys. Lett.* **414**, 117–121 (2005).
11. Nakai, K., Kato, T., Kono, H. & Yamanouchi, K. Communication: long-lived neutral H_2 in hydrogen migration within methanol dication. *J. Chem. Phys.* **139**, 181103 (2013).

12. Okino, T. et al. Ejection dynamics of hydrogen molecular ions from methanol in intense laser fields. *J. Phys. B. At. Mol. Opt. Phys.* **39**, S515–S521 (2006).
13. Okino, T. et al. Coincidence momentum imaging of ejection of hydrogen molecular ions from methanol in intense laser fields. *Chem. Phys. Lett.* **419**, 223–227 (2006).
14. Kanya, R. et al. Hydrogen scrambling in ethane induced by intense laser fields: statistical analysis of coincidence events. *J. Phys. Chem.* **136**, 204309 (2012).
15. Karlsson, L., Jadrny, R., Mattsson, L., Chau, F. T. & Siegbahn, K. Vibrational and vibronic structure in the valence electron spectra of CH_3X molecules (X=F, Cl, Br, I, OH). *Phys. Scr.* **16**, 225–234 (1977).
16. Borkar, S., Sztáray, B. & Bodi, A. Dissociative photoionization mechanism of methanol isotopologues (CH_3OH, CD_3OH, CH_3OD and CD_3OD) by iPEPICO: energetics, statistical and non-statistical kinetics and isotope effects. *Phys. Chem. Chem. Phys.* **13**, 13009–13020 (2011).
17. Eland, J. H. D. & Treves-Brown, B. J. The fragmentation of doubly charged methanol. *Int. J. Mass Spectrom. Ion. Process.* **113**, 167–176 (1992).
18. Kimura, K. & Kubo, M. Structures of dimethyl ether and methyl alcohol. *J. Chem. Phys.* **30**, 151–158 (1959).
19. Thapa, B. & Schlegel, H. B. Molecular dynamics of methanol monocation (CH_3OH^+) in strong laser fields. *J. Phys. Chem. A* **118**, 1769–1776 (2014).
20. Laidler, K. J. *Chemical Kinetics* 3rd edn (HarperCollins, New York, 1987).
21. Macneil, K. A. G. & Dixon, R. N. High-resolution photoelectron spectroscopy of methanol and its deuterated derivatives: internal rotation in the ground ionic state. *J. Electr. Spectr. Rel. Phen.* **11**, 315–331 (1977).
22. Ando, T. et al. Wave packet bifurcation in ultrafast hydrogen migration in CH_3OH^+ by pump-probe coincidence momentum imaging with few-cycle laser pulses. *Chem. Phys. Lett.* **624**, 78–82 (2015).
23. Birge, J. R., Ell, R. & Kärtner, F. X. Two-dimensional spectral shearing interferometry for few-cycle pulse characterization. *Opt. Lett.* **31**, 2063–2065 (2006).
24. Hasegawa, H., Hishikawa, A. & Yamanouchi, K. Coincidence imaging of Coulomb explosion of CS_2 in intense laser fields. *Chem. Phys. Lett.* **349**, 57–63 (2001).
25. Frasinski, L. J., Codling, K. & Hatherly, P. A. Covariance mapping method applied to multiphoton multiple ionization. *Science* **246**, 1029–1031 (1989).
26. K. Ohno, K. & Maeda, S. A scaled hypersphere search method for the topography of reaction pathways on the potential energy surface. *Chem. Phys. Lett.* **384**, 277–282 (2004).
27. Maeda, S. & Ohno, K. Global mapping of equilibrium and transition structures on potential energy surfaces by the scaled hypersphere search method: applications to ab initio surfaces of formaldehyde and propyne molecules. *J. Phys. Chem. A* **109**, 5742–5753 (2005).
28. Ohno, K. & Maeda, S. Global reaction route mapping on potential energy surfaces of formaldehyde, formic acid, and their metal-substituted analogues. *J. Phys. Chem. A* **110**, 8933–8941 (2006).
29. Beyer, T. & Swinehart, D. F. Algorithm 448: number of multiply-restricted partitions. *Commun. Acm.* **16**, 379 (1973).

Acknowledgements

The present research was supported by the following three grants from the Ministry of Education, Culture, Sports, Science and Technology (MEXT), Japan: two Grant-in-Aid for Specially Promoted Research (#19002006 and #15H05696) and a Grant-in-Aid for Scientific Research A (#24245003).

Author contributions

T.A., A.S., S.M. and A.I., developed the experimental method. T.A. performed the experiments. T.A. and K.Y. analyzed the data. K.N. performed the GRRM calculations. The manuscript was prepared by T.A. and K.Y., and was discussed among all authors.

Additional information

Supplementary information is available for this paper at https://doi.org/10.1038/s42004-017-0006-7.

Competing interests: The authors declare no competing financial interests.

Reprints and permission information is available online at http://npg.nature.com/reprintsandpermissions/

Publisher's note: Springer Nature remains neutral with regard to jurisdictional claims in published maps and institutional affiliations.